Published in final edited form as:
Ann Neurol. 2014 September ; 76(3): 370–378. doi:10.1002/ana.24213.

In-Vivo Imaging of Spinal Cord Atrophy in Neuroinflammatory Diseases

Winston Liu[1,2,*], **Govind Nair**[1,*], **Luisa Vuolo**[1], **Anshika Bakshi**[1,3], **Raya Massoud**[1], **Daniel S. Reich**[1], and **Steven Jacobson**[1]

[1]Neuroimmunology Branch, National Institute of Neurological Disorders and Stroke, Bethesda, MD, USA

[2]Fischell Department of Bioengineering, University of Maryland, College Park, MD, USA

[3]Tufts University School of Medicine, Boston, MA, USA

Abstract

Objective—Spinal cord atrophy is prominent in chronic progressive neurologic diseases such as Human-T-cell lymphotropic virus type-1 (HTLV-1) associated myelopathy/tropical spastic paraparesis (HAM/TSP) and multiple sclerosis (MS). Here we compared the spinal cord cross-sectional area (SCCSA) in HAM/TSP and MS to that of healthy volunteers (HV).

Methods—SCCSA and clinical disability scores were measured in 18 HAM/TSP, 4 asymptomatic carriers (AC) of HTLV-1, 18 MS, and 10 HV from a 3T MRI. SCCSA measured in patients and AC were compared to that of HV and correlated with disability scores.

Results—The entire spinal cord in HAM/TSP was thin compared to HV, whereas only the cervical cord in MS was thinner than HV ($p<0{\cdot}0001$). In HAM/TSP, SCCSA extensively correlated with Ambulation Index, whereas only the cervical cord correlated with disease duration ($p<0{\cdot}05$). In MS, the SCCSA extensively correlated with Scripps Neurologic Rating Score and the Expanded Disability Status Scale ($p<0{\cdot}05$). One of the four ACs showed atrophy in a pattern similar to HAM/TSP.

Interpretation—These results are in accordance with the findings that whereas over half of all lesions in an MS cord are seen in the upper cervical cord, most of the pathology in HAM/TSP is seen in the thoracolumbar cord, which in turn may be responsible for more extensive cord atrophy seen in HAM/TSP. Imaging marker such as SCCSA might serve as a surrogate endpoint in clinical trials, especially to assess the neuroprotective impact of various therapies.

Corresponding author: Steven Jacobson, National Institute of Neurological Disorders and Stroke, National Institutes of Health, Bldg 10, Rm 5C103, 10 Center Drive, MSC 1400, Bethesda, MD 20892, USA. jacobsons@mail.nih.gov.
*These authors contributed equally to this work.

Author contributions

All authors analyzed and interpreted the data and participated in writing and revising the manuscript. All authors approve the final version of the report, and vouch for the integrity of the data and analyses. Authors GN, DSR, and SJ conceived and designed the study. Authors GN and WL created and debugged the algorithm. Authors WL, AB, LV generated the patient data and ran statistics. Author RM acquired the clinical data used in the paper.

Keywords

HTLV-1 associated myelopathy/tropical spastic paraparesis (HAM/TSP); Multiple sclerosis (MS); Magnetic resonance imaging (MRI); Spinal cord; Atrophy

INTRODUCTION

Atrophy of the brain and spinal cord is a prominent MRI finding in inflammatory central nervous system diseases. Loss of volume on MRI is thought to reflect the most destructive pathological processes in these diseases, including irreversible demyelination and loss of astroglia, neuronal cell bodies, and axons.

About 3% of individuals infected with Human-T-cell lymphotropic virus type-1 (HTLV-1) (1) develop a relentlessly progressive myelopathy termed HTLV-1 associated myelopathy/ tropical spastic paraparesis (HAM/TSP) (2). Clinical manifestations of HAM/TSP include a predominance of pyramidal deficits in the lower extremities as well as bowel and bladder dysfunction. Axonal loss and demyelination, with the former gradually predominating, are observed on histopathology (3, 4). Lesions seen in the mid to lower thoracolumbar spinal cord are the most severe and account for the main clinical symptoms, with predominant involvement of the lateral columns and cord atrophy (4–7). However, measurement of spinal cord atrophy is still suboptimal in HAM/TSP.

Multiple sclerosis (MS) is a chronic inflammatory, demyelinating, and neurodegenerative disease of the central nervous system. Atrophy is an early finding in MS that worsens with the progression of disability and correlates better with clinical disability than do conventional measures of the inflammatory process, such as lesion count and volume (8). In particular, cervical spinal cord atrophy is well studied quantitatively in MS and has been shown to correlate with relevant clinical measures; measurement of cervical atrophy is therefore considered to be a promising measure for treatment assessment in clinical practice and trials (9–11).

The conventional method for detecting cord atrophy is through visual examination of MRI by a trained radiologist. In HAM/TSP, this binary approach generally results in detecting a <40% incidence of thin cords, but the extent of that atrophy is not quantified (5, 12, 13). Computer-driven measurements of atrophy have used spinal cord cross-sectional area (SCCSA) as an indicator for atrophy (9, 14–16). These measurements were traditionally conducted through manually drawn regions of interests (ROIs) at specific levels (9, 17). However, in diseases where the topography of cord involvement is unknown, analysis at specific levels can bias results. Thus, for a better understanding of the macroscopic disease manifestation in the spinal cord, it is imperative to develop better techniques to detect continuous profiles of SCCSA along the length of the entire spinal cord.

Recent advances in atrophy quantification have involved better imaging protocols with higher resolution (18) and image contrast (19–21), as well as enhanced post-processing methods (14, 22). However, semi-automatic methods are often time consuming and require substantial manual input. In addition, most studies have focused on quantifying changes in

the cervical cord, where there are fewer motion artifacts, and changes in the thoracolumbar cord have been underemphasized. The goal of this study was to map SCCSA profiles along the length of the entire spinal cord in HAM/TSP and to compare the results with MS and healthy volunteers (HV). We also examined the relationship between SCCSA and clinical disability measures in HAM/TSP and MS to determine if this measure could potentially serve as a surrogate marker of disability.

METHODS

Subjects

MRI of the cervical and thoracolumbar spinal cord was performed on 20 subjects with the diagnosis of HAM/TSP according to the published WHO diagnostic criteria, five subjects with asymptomatic HTLV-1 infection (AC, spouses of patients with HAM/TSP), 20 subjects clinically diagnosed with MS and ten healthy volunteers. Written, informed consent was obtained from all participants, and the Institutional Review Board at the National Institutes of Health approved all protocols.

Clinical disability in HAM/TSP patients was measured using the Instituto de Pesquisas de Cananeia (IPEC) score, Kurtzke's Expanded Disability Status Scale (EDSS), Scripps Neurologic Rating Score (SNRS), and the Hauser Ambulation Index (AI). HTLV-1 proviral load (PVL) was measured using digital droplet PCR. Measures of clinical disability in the MS patients included only the EDSS and SNRS scores.

MR Image Acquisition

MR imaging was performed on a 3T Skyra system (Siemens, Malvern, PA) equipped with a 20-channel head-neck coil and a 16-channel spine-array coil. T1-weighted images were acquired in the cervical spine using 3D-gradient-echo sequences with FOV = 256 mm, TR = 7·8 ms, TE = 3 ms, 1 mm isotropic resolution, 16° flip angle, and GRAPPA=2, for a scan time of about 3 min 30 seconds. The sequence was repeated for the thoracic spine, which contains the thoracolumbar cord, by changing the FOV and base resolution to 320 mm in order to cover the larger anatomy while maintaining the 1 mm isotropic resolution. Additional sequences were also used in the cervical and thoracolumbar regions including short tau inversion recovery (STIR), T2-weighted, T1-MPRAGE, and axial gradient echo.

MR Image Analysis

The cervical and thoracolumbar spine images were stitched together using their DICOM information, and AFNI functions and were further analyzed as a single image. SCCSA calculation algorithm was written in MATLAB. Briefly, user defined rotation with R-L and I-S axes was carried out to bring the entire cord into a mid-sagittal plane. Next, all the edges on the user-selected mid-sagittal image were detected using the Canny method (23), from which the user selected the edge corresponding to the spinal cord by clicking the superior (level of the tip of the odontoid process) and inferior (T10 – T11 disc, cyan line in Figure 1a) aspects. The algorithm then reformated a 40×40mm square image perpendicular to each point along the cord-edge (by defining the cord edge as a polynomial) and selected the edge closest to or intersecting the sagittal polynomial as enclosing the spinal cord (red contour in

Figure 1b). The area enclosed by the polynomial was taken to be the SCCSA at that point (Figure 1c), and the process was repeated automatically for the length of the cord. The SCCSA profile was defined as the plot of SCCSA as a function of the percentage-distance along the cord from the C1 to T10 vertebral bodies. In addition, the average positions of each vertebral body segments were also noted in the HV group and plotted as vertical dotted lines on the SCCSA plots.

Cord detection was deemed to have failed when the edge of the cord could not be detected in the sagittal plane or when SCCSA could not be detected in more than 40% of axial reformatted planes along the cord. Incorrectly measured areas were defined as planes where the area changed more than 25% from the previously correctly measured area, where more than 50% of the points in the detected region were not in the previously correctly measured region, or where the enclosed points were not hyperintense as compared to points just outside the region in the T1-weighted scans.

Statistical Analysis

All values are expressed in mean ± SD except where noted. SCCSAs were averaged within each vertebral body segment. A pairwise Tukey range test was used in conjunction with ANOVA to assess the differences between the groups with covariates of age and sex. Multiple regressions were used to assess relationships between clinical measures and SCCSA with adjustment for age, sex, and multiple comparisons. A p-value of <0·05 was considered significant.

RESULTS

Clinical Demographics

SCCSA profiles were successfully measured in 50 out of 55 subjects recruited for this study (10 out of 10 HV, 18 out of 20 HAM/TSP, 18 out of 20 MS, and 4 out of 5 AC). Demographic information and clinical characteristics of these subjects are summarized in Table 1.

Spinal Cord Patterns Vary by Disease Group

Figure 2 shows the SCCSA profile plots from HV (blue), HAM/TSP (green), and MS (red) subjects. In the HV group, the mean SCCSA from cervical and thoracolumbar regions were 72·0 ± 6 mm^2 and 38·8 ± 6 mm^2, respectively. Average SCCSA in HAM/TSP was significantly lower ($p \ll 0{\cdot}001$) in both the cervical (50·8 ± 10 mm^2) and thoracolumbar (24·8 ± 5 mm^2) regions compared to HV. Similarly, average SCCSA in MS (57·4 ± 10 mm^2) was significantly lower ($p < 0{\cdot}001$; Fig 2, red vs. blue) but only approached significance ($p = 0{\cdot}11$) in thoracolumbar region (34·1 ± 6 mm^2) when compared to HV. In the thoracolumbar region, SCCSA was significantly (pLt;0·001) smaller in HAM/TSP compared to MS, but this was not the case in the cervical region (p=0·1).

The location of vertebral body segments as a percentage of the length of the entire cord (C1–T10 vertebral bodies) was found to be relatively consistent amongst the HV. The C7 segment ended consistently at 32 ± 1% of the total cord length. Likewise, all other cord

segment locations were within 2 x SD in our subject cohort (vertical lines with SEM red line in Figure 2).

A significant difference was detected across the three disease groups in all regions defined through segment locations (ANOVA F-test, $p \ll 0{\cdot}001$). HAM/TSP SCCSA was less than HV SCCSA throughout the analyzed cord (C1–T10 vertebral bodies, $p < 0{\cdot}001$), ranging from 75% of the mean HV SCCSA at C3, decreasing to 59% at T4, and increasing to 67% at T9. However, MS SCCSA ranged from 78% of mean HV SCCSA in the C4–C6 region to 97% of the HV SCCSA at T10 and was significantly smaller only in the cervical region. HAM/TSP SCCSA differed from MS SCCSA predominantly in the thoracolumbar cord (C7–T10 vertebral body levels, $p<0{\cdot}05$) and at the level of the C1 vertebral body.

Reliability of the Measure

Five healthy volunteers returned for a second scan within six months (145 ± 49 days). Bland-Altman plots showed that differences between the two scans were distributed around zero and that there was no bias (Figure 3). Mean absolute difference in average SCCSA between the two scans was 0·50 mm^2 in the whole spine (ICC: 0.99), 1·17 mm^2 in the cervical spine (ICC: 0·95) and 1·25 mm^2 in the thoracolumbar spine (ICC: 0·92).

Clinical Correlates with SCCSA

Age adjusted Pearson's partial *r* coefficients for clinical disability scores with SCCSA of cervical cord, thoracolumbar cord, and individual vertebral body segments are shown in Table 2.

Asymptomatic Carriers

Whereas two ACs (AC-1, -2) had SCCSAs profiles that fit within the HV range (Figure 4, average Z-score from HV of 0·01 and −0·58), AC-3 had a SCCSA that was more like the HAM/TSP group (average Z-score from HV of −2·88). AC-4 had a SCCSA profile that was more atrophic than typical HV but less than HAM/TSP (Figure 4). Of note, the AC-3 with smaller SCCSA had a high HTLV-I proviral load (45·5%), whereas the other 3 ACs had typically low proviral loads (<2%).

DISCUSSION

In this study, the SCCSA in HAM/TSP and MS was found to be lower than in age-matched HV. Interestingly, the pattern of atrophy was different between the two disease groups, and this pattern was easily visualized with the novel analysis technique reported herein. On average, the entire length of the cord was atrophic in HAM/TSP, whereas only the cervical cord atrophic in MS. Importantly, clinical measures of disability were correlated with SCCSA in both HAM/TSP and MS, with SCCSA showing significant correlations with specific clinical measures of motor disability in the HAM/TSP group. Finally, analysis of individual SCCSA from 4 HTLV-I ACs showed wide variations, from cords that looked similar to HV to one that closely resembled the average SCCSA pattern seen in the HAM/TSP group. Such analysis of the patterns of SCCSA along its entire length has the

utility to monitor the natural history of spinal cord atrophy patterns with more sensitivity than single or multiple measurements at various levels of the cord.

Previous studies have used the ratio between cord and spinal canal size at certain levels to estimate atrophy in HAM/TSP, but such indices have not been shown to have a strong relationship with disease progression and are strongly affected by the chosen slice as well as the extent of degenerative disease in the spine (24, 25). A recently reported technique quantifying cervical and thoracolumbar spinal cord volume also showed significant differences between HAM/TSP and HV (15). However, the sample size was very small, and the described technique required significant user input and manual correction. Furthermore, the length of an individual's spinal cord confounds the use of volume, favoring the use of SCCSA (16, 21). Spinal cord analyses in MS have traditionally relied on ROIs at specific levels (9, 26) and more recently on active-surface models (14, 22). Our technique looks at the SCCSA at each point along the entire spinal cord instead of fitting the cord to a cylinder as in the active-surface model, making it potentially more sensitive to local changes.

SCCSA reduction in the cervical cord of MS patients reported herein is consistent with reports using an active-surface method (27–29). Differences in cervical SCCSA have primarily been reported in progressive MS but not in relapsing remitting (30) or clinically isolated syndrome (27). In the small MS cohort included in this study, most had relapsing-remitting MS, and even in this group we detected significant cord atrophy using our analysis technique. Further cross-sectional studies with larger numbers of MS patients stratified by subtypes are in progress.

Correlations between this measure of atrophy and clinical disability scores in both HAM/TSP and MS confirm that SCCSA is a clinically relevant index. Interestingly, HAM/TSP SCCSA correlated more strongly with scores that are more heavily weighted toward ambulation, including EDSS and particularly the AI (an ordinal scale based on the 25 foot timed walk), than with more general clinical disability scores such as SNRS and IPEC. In HAM/TSP, significant correlation between spinal cord atrophy and ambulatory disability highlights the need to explore more specific clinical measures of motor disability such as finger and foot tapping speeds. Axonal degeneration along the spinal cord may play a more prominent role in disease progression in HAM/TSP and may explain the significant correlation seen between SCCSA and disease duration.

It is generally reported that high HTLV-I proviral load is a risk factor for HAM/TSP (i.e., higher PVL in HAM/TSP patients than in asymptomatic carriers), yet in this study there was no correlation between HTLV-I PVL and the degree of spinal cord atrophy. This result is consistent with previous findings that HTLV-I PVL remains stable despite the progression of disability in most HAM/TSP cases and suggests that disability progression is due to neurodegeneration and irreversible tissue loss (31). Thus, antiviral therapies that reduce PVL might not be sufficient to arrest disability progression. This study did not assess whether PVL or other inflammatory markers in the cerebrospinal fluid may be a better correlate of HAM/TSP spinal cord atrophy.

Since the vast majority of HTLV-I infected individuals are asymptomatic, it was of interest to determine the SCCSA in these cases. In most studies, particularly in non-endemic areas, these asymptomatic carriers are rarely evaluated. Two AC had SCCSA measurements within normal HV values, one was intermediate between HAM/TSP and HV, and one had spinal cord atrophy in a pattern similar to HAM/TSP. While our study uncovered SCCSA differences between HAM/TSP and HV as well as correlation between SCCSA and clinical disability, it should be noted that SCCSA measured at a single time point in an individual cannot be taken as an accurate measure of atrophy due to intersubject variability in baseline SCCSA. At the same time, the results of this study suggest that SCCSA substantially smaller than typical HV values most likely suggests that atrophy as occurred. Furthermore, these observations highlight the need to expand these studies to larger cohorts of patients and carriers, particularly in endemic areas where sufficient numbers of subjects can be recruited to validate the diagnostic and prognostic value of these novel radiological measurements. To further our understanding of disease manifestation and progression, subjects in the AC group will be longitudinally followed in the clinic and with MRI.

It should be noted that SCCSA algorithm failed in 2 of 20 HAM/TSP and MS patients, as well as in 1 of 5 ACs. The area calculation in a patient was taken to have failed if the area was not detected in more than 40% of the length of the cord. Such failures often occurred due to artifacts such as blurring due to motion, or a lack of contrast between the cord and the cerebrospinal fluid (such as in cord stenosis), which lead to failures in edge detection. However, the constraints used in our technique prevent an artifact in a particular a region of low contrast from distorting measurements in normal regions. In cases where area was determined in more than 60% of the length of the cord, the complete profile plots were created by one-dimensional interpolation of the profile data. Other approaches, such as image filtering or enhancing techniques (such as anisotropic diffusion filtering) may further improve the reliability of edge detection.

Distances along the cord were normalized to the cord length, and we found that the vertebral body segments fall very tightly in the cohort that we tested. However, it should be noted that the vertebral level-wise analysis reported herein does not inform directly about the cord segment. Automatic detection of cord segments is far more challenging due to the small size of exiting nerve roots at each level and to artifacts associated with spinal cord motion. On the other hand, the high-contrast boundaries of the intervertebral disks, easily visible on the mid-sagittal slice, helped to define reliable regions for segmentation on the cord for analysis. In addition, the SCCSA was analyzed in the portion of the cord between the C1 and T10 vertebral bodies and in general did not extend to the lumbar enlargement; this restriction was done to achieve uniformity between patients and to limit failures of edge detection due to the cauda equina. In our cohort, 7 subjects had a discernible lumbar enlargement at vertebral body level T11, 36 at T12, and 3 at L1. This variability may further confound any correlations with clinical disability relating to gait such as AI. Other techniques such as normalizing the SCCSA to the length of the cord (from the cervicomedullary junction to the conus medullaris) or examining the region of the lumbar enlargement alone can be proposed to further develop MRI markers of the clinical disabilities with gait.

We plan to use the novel algorithm in longitudinal studies to detect changes in spinal SCCSA over time in order to better understand its relation to disease progression. With larger subject cohorts and prospective longitudinal studies, the novel approach may help to clarify disease progression and could potentially serve as a surrogate endpoint in clinical trials.

Acknowledgments

Kory Johnson and Tianxia Wu for their help with some of the statistics. Funded by the intramural research program at NIH.

References

1. Poiesz BJ, Ruscetti FW, Gazdar AF, Bunn PA, Minna JD, Gallo RC. Detection and isolation of type C retrovirus particles from fresh and cultured lymphocytes of a patient with cutaneous T-cell lymphoma. Proc Natl Acad Sci U S A. 1980 Dec; 77(12):7415–9. [PubMed: 6261256]
2. Proietti FA, Carneiro-Proietti AB, Catalan-Soares BC, Murphy EL. Global epidemiology of HTLV-I infection and associated diseases. Oncogene. 2005 Sep 5; 24(39):6058–68. Epub 2005/09/13. eng. [PubMed: 16155612]
3. Umehara F, Izumo S, Nakagawa M, Ronquillo AT, Takahashi K, Matsumuro K, et al. Immunocytochemical analysis of the cellular infiltrate in the spinal cord lesions in HTLV-I-associated myelopathy. Journal of neuropathology and experimental neurology. 1993 Jul; 52(4): 424–30. [PubMed: 8355031]
4. Aye MM, Matsuoka E, Moritoyo T, Umehara F, Suehara M, Hokezu Y, et al. Histopathological analysis of four autopsy cases of HTLV-I-associated myelopathy/tropical spastic paraparesis: inflammatory changes occur simultaneously in the entire central nervous system. Acta neuropathologica. 2000 Sep; 100(3):245–52. [PubMed: 10965793]
5. Bagnato F, Butman JA, Mora CA, Gupta S, Yamano Y, Tasciyan TA, et al. Conventional magnetic resonance imaging features in patients with tropical spastic paraparesis. Journal of neurovirology. 2005 Dec; 11(6):525–34. [PubMed: 16338746]
6. Kermode AG, Rudge P, Thompson AJ, du Boulay EP, McDonald WI. MRI of thoracic cord in tropical spastic paraparesis. Journal of neurology, neurosurgery, and psychiatry. 1990 Dec; 53(12): 1110–1.
7. Melo A, Moura L, Rios S, Machado M, Costa G. Magnetic resonance imaging in HTLV-I associated myelopathy. Arquivos de neuro-psiquiatria. 1993 Sep; 51(3):329–32. [PubMed: 8297235]
8. Miller DH, Barkhof F, Frank JA, Parker GJ, Thompson AJ. Measurement of atrophy in multiple sclerosis: pathological basis, methodological aspects and clinical relevance. Brain : a journal of neurology. 2002 Aug; 125(Pt 8):1676–95. [PubMed: 12135961]
9. Losseff NA, Webb SL, O'Riordan JI, Page R, Wang L, Barker GJ, et al. Spinal cord atrophy and disability in multiple sclerosis. A new reproducible and sensitive MRI method with potential to monitor disease progression. Brain : a journal of neurology. 1996 Jun; 119(Pt 3):701–8. [PubMed: 8673483]
10. Lin X, Tench CR, Turner B, Blumhardt LD, Constantinescu CS. Spinal cord atrophy and disability in multiple sclerosis over four years: application of a reproducible automated technique in monitoring disease progression in a cohort of the interferon beta-1a (Rebif) treatment trial. Journal of neurology, neurosurgery, and psychiatry. 2003 Aug; 74(8):1090–4.
11. Horsfield MA, Filippi M. Spinal cord atrophy and disability in multiple sclerosis over four years. Journal of neurology, neurosurgery, and psychiatry. 2003 Aug; 74(8):1014–5.
12. Milagres AC, Jorge ML, Marchiori PE, Segurado AA. Human T cell lymphotropic virus type 1-associated myelopathy in Sao Paulo, Brazil. Epidemiologic and clinical features of a university hospital cohort. Neuroepidemiology. 2002 May-Jun;21(3):153–8. [PubMed: 12006779]

13. Alcindor F, Valderrama R, Canavaggio M, Lee H, Katz A, Montesinos C, et al. Imaging of human T-lymphotropic virus type I-associated chronic progressive myeloneuropathies. Neuroradiology. 1992; 35(1):69–74. [PubMed: 1289743]
14. Horsfield MA, Sala S, Neema M, Absinta M, Bakshi A, Sormani MP, et al. Rapid semi-automatic segmentation of the spinal cord from magnetic resonance images: application in multiple sclerosis. NeuroImage. 2010 Apr 1; 50(2):446–55. [PubMed: 20060481]
15. Evangelou IE, Massoud R, Jacobson S. HTLV-I-associated myelopathy/tropical spastic paraparesis: semiautomatic quantification of spinal cord atrophy from 3-dimensional MR images. Journal of neuroimaging : official journal of the American Society of Neuroimaging. 2014 Jan-Feb;24(1):74–8. [PubMed: 22303896]
16. Oh J, Zackowski K, Chen M, Newsome S, Saidha S, Smith SA, et al. Multiparametric MRI correlates of sensorimotor function in the spinal cord in multiple sclerosis. Multiple sclerosis. 2013 Apr; 19(4):427–35. [PubMed: 22891033]
17. Kidd D, Thorpe JW, Thompson AJ, Kendall BE, Moseley IF, MacManus DG, et al. Spinal cord MRI using multi-array coils and fast spin echo. II. Findings in multiple sclerosis. Neurology. 1993 Dec; 43(12):2632–7. [PubMed: 8255468]
18. Sigmund EE, Suero GA, Hu C, McGorty K, Sodickson DK, Wiggins GC, et al. High-resolution human cervical spinal cord imaging at 7 T. NMR in biomedicine. 2012 Jul; 25(7):891–9. [PubMed: 22183956]
19. Kearney H, Yiannakas MC, Abdel-Aziz K, Wheeler-Kingshott CA, Altmann DR, Ciccarelli O, et al. Improved MRI quantification of spinal cord atrophy in multiple sclerosis. Journal of magnetic resonance imaging : JMRI. 2014 Mar; 39(3):617–23. [PubMed: 23633384]
20. Nair G, Absinta M, Reich DS. Optimized T1-MPRAGE sequence for better visualization of spinal cord multiple sclerosis lesions at 3T. AJNR American journal of neuroradiology. 2013 Nov-Dec; 34(11):2215–22. [PubMed: 23764721]
21. Bakshi R, Thompson AJ, Rocca MA, Pelletier D, Dousset V, Barkhof F, et al. MRI in multiple sclerosis: current status and future prospects. Lancet neurology. 2008 Jul; 7(7):615–25.
22. Chen M, Carass A, Oh J, Nair G, Pham DL, Reich DS, et al. Automatic magnetic resonance spinal cord segmentation with topology constraints for variable fields of view. NeuroImage. 2013 Dec. 83:1051–62. [PubMed: 23927903]
23. Canny J. A computational approach to edge detection. IEEE transactions on pattern analysis and machine intelligence. 1986 Jun; 8(6):679–98. [PubMed: 21869365]
24. Ferraz AC, Gabbai AA, Abdala N, Nogueira RG. Magnetic resonance in HTL-I associated myelopathy. Leukoencephalopathy and spinal cord atrophy. Arquivos de neuro-psiquiatria. 1997 Dec; 55(4):728–36. Ressonancia magnetica na mielopatia associada ao HTLV-I. Leucoencefalopatia e atrofia medular. [PubMed: 9629331]
25. Yukitake M, Takase Y, Nanri Y, Kosugi M, Eriguchi M, Yakushiji Y, et al. Incidence and clinical significances of human T-cell lymphotropic virus type I-associated myelopathy with T2 hyperintensity on spinal magnetic resonance images. Internal medicine. 2008; 47(21):1881–6. [PubMed: 18981631]
26. Lin X, Tench CR, Evangelou N, Jaspan T, Constantinescu CS. Measurement of spinal cord atrophy in multiple sclerosis. Journal of neuroimaging : official journal of the American Society of Neuroimaging. 2004 Jul; 14(3 Suppl):20S–6S. [PubMed: 15228756]
27. Klein JP, Arora A, Neema M, Healy BC, Tauhid S, Goldberg-Zimring D, et al. A 3T MR imaging investigation of the topography of whole spinal cord atrophy in multiple sclerosis. AJNR American journal of neuroradiology. 2011 Jun-Jul;32(6):1138–42. [PubMed: 21527570]
28. Rocca MA, Horsfield MA, Sala S, Copetti M, Valsasina P, Mesaros S, et al. A multicenter assessment of cervical cord atrophy among MS clinical phenotypes. Neurology. 2011 Jun 14; 76(24):2096–102. [PubMed: 21670439]
29. Valsasina P, Rocca MA, Horsfield MA, Absinta M, Messina R, Caputo D, et al. Regional cervical cord atrophy and disability in multiple sclerosis: a voxel-based analysis. Radiology. 2013 Mar; 266(3):853–61. [PubMed: 23192778]

30. Sena A, Pedrosa R, Ferret-Sena V, Cascais MJ, Roque R, Araujo C, et al. Interferon beta therapy increases serum ferritin levels in patients with relapsing-remitting multiple sclerosis. Multiple sclerosis. 2008 Jul; 14(6):857–9. [PubMed: 18573825]

31. Olavarria VN, Gomes Ado N, Kruschewsky Rde A, Galvao-Castro B, Grassi MF. Evolution of HTLV-1 proviral load in patients from Salvador, Brazil. The Brazilian journal of infectious diseases : an official publication of the Brazilian Society of Infectious Diseases. 2012 Jul-Aug; 16(4):357–60.

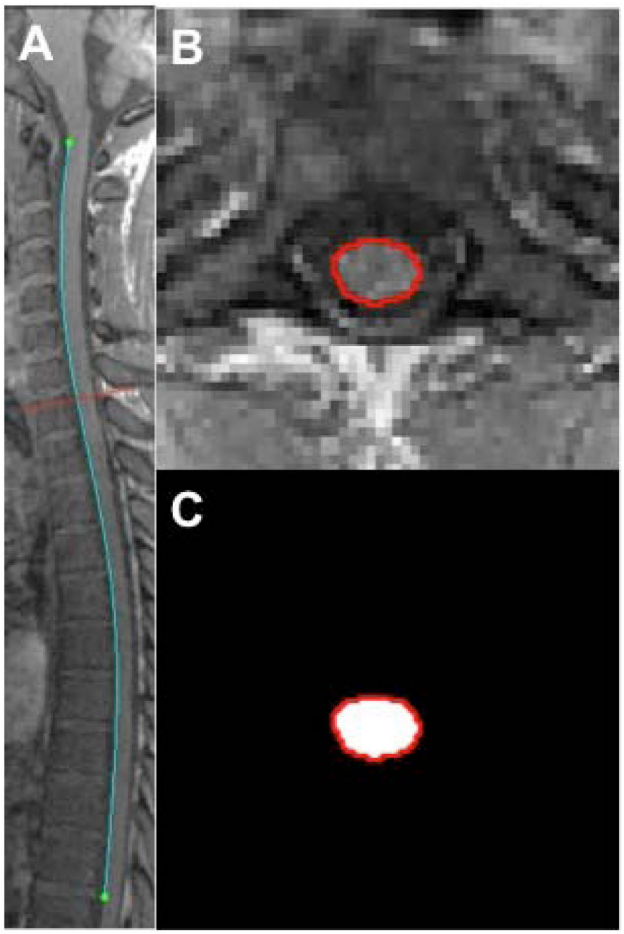

Figure 1.

(A) Representative mid-sagittal T1-weighted MRI of the cervical and thoracolumbar cord from a 26 year-old, female HAM/TSP patient. Separate cervical and thoracolumbar scans were stitched together using scanner-provided information on slice position and angulation. Edges within the image were automatically detected; an operator than manually selected the upper and lower extent of the edge corresponding to the spinal cord (in blue). (B) Representative axial images (along the red line in A) reconstructed perpendicular to the blue line in A. The cord edge (red line in B) was detected as the edge in B that also intersects the blue line in A. (C) The area inside the polygonal contour (cord edge) is calculated automatically, and the process is repeated at each point along the cord (blue line in A).

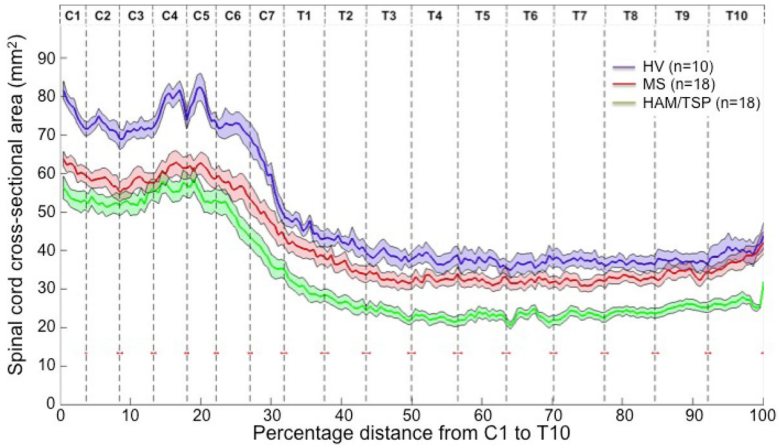

Figure 2.

Profile of the cross-sectional area along the length of the spinal cord (mean: dark line, standard error of the mean: shaded region) in healthy volunteers (blue; n=10), multiple sclerosis (MS; red; n=18), and HTLV-I associated myelopathy/tropical spastic paraparesis (HAM/TSP; green; n=18). Results of pairwise Tukey Honestly Significant Difference (HSD) tests are shown above the graph (one symbol: $p<0{\cdot}025$, two symbols: $p<0{\cdot}001$).

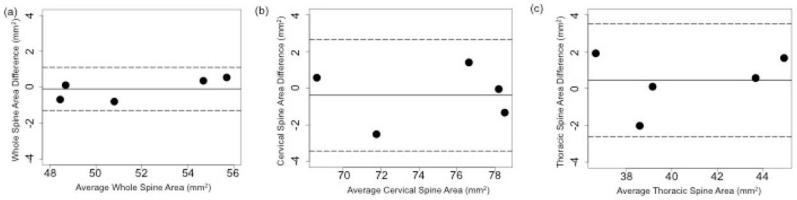

Figure 3.

Difference in spinal cord cross-sectional area (SCCSA) between two scans performed an average four months apart from (A) average SCCSA across the whole spine; (B) average cervical SCCSA; and (C) average thoracolumbar SCCSA. Dotted lines indicate 95% confidence intervals.

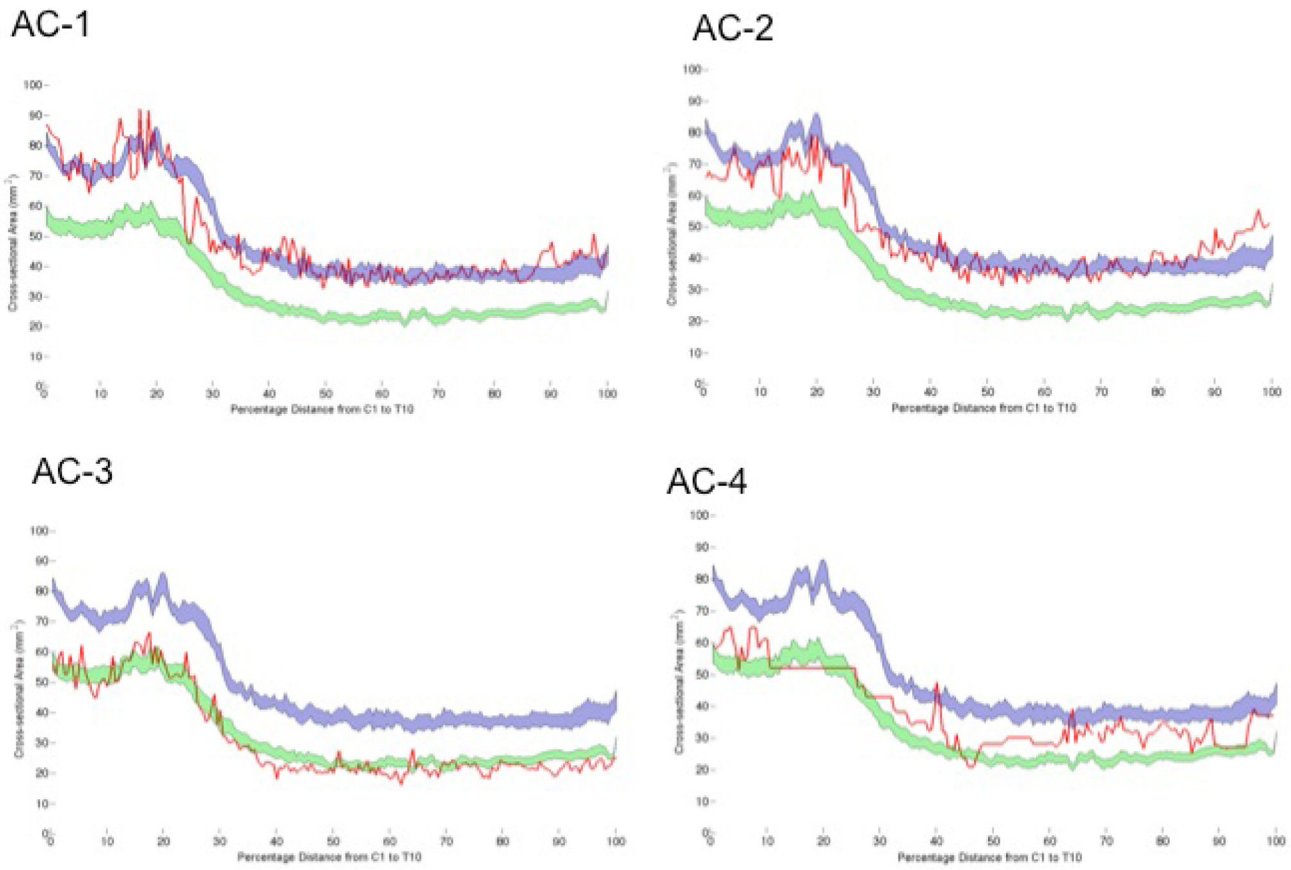

Figure 4.

Spinal cord cross-sectional area (SCCSA) profile from 4 HTLV-I asymptomatic carriers (AC1 - AC4, red lines) overlaid on group-averaged healthy-volunteer SCCSA (blue region) and HAM/TSP SCCSA (green region) from Figure 2. SCCSA profile in AC-1 and AC-2 closely matched the healthy volunteer pattern (Z-scores relative to healthy volunteers: 0·01 and −0·58), whereas the SCCSA profile in AC-3 was similar to HAM/TSP patients (Z-score: −2·88). AC-4 had an intermediate profile between healthy volunteers and HAM/TSP.

Table 1

Patient demographics and clinical disability scores by disease type. EDSS Expanded Disability Status Scale, SNRS Scripps Neurologic Rating Score, IPEC the Instituto de Pesquisas de Cananeia score, DD disease duration, AI Hauser Ambulation Index.

Diagnosis	*n*	Age (years) Mean ± SD	Gender m-f	EDSS Med (IQR)	SNRS Med (IQR)	IPEC Med (IQR)	DD (years) Mean ± SD	AI Med (IQR)
HV	10	46 ± 8	2-8	---	---	---	---	---
HAM/TSP	18	52 ± 12	7-11	6.5 (1)	56 (14)	15 (8.5)	11 ± 7	5 (2)
MS	18	47 ± 11	10-8	6 (4.9)	75 (28)	---	16 ± 11	---
AC	4	54 ± 10	0-4	---	---	---	---	---

Table 2

Pearson's partial correlation coefficients between spinal cord cross-sectional area at various vertebral levels with clinical disability scores, adjusted for age in HAM/TSP and MS. Shaded region = $p<0.05$. SNRS Scripps Neurologic Rating Score, EDSS Expanded Disability Status Scale, IPEC the Instituto de Pesquisas de Cananeia score, DD disease duration, AI Hauser Ambulation Index, and PVL Proviral load.

HAM/TSP (*n*=18)	C1	C2	C3	C4	C5	C6	C7	T1	T2	T3	T4	T5	T6	T7	T8	T9	T-10	C	T
SNRS	0.14	0.14	0.22	0.24	0.09	0.22	0.16	0.29	0.20	0.14	0.22	0.18	0.25	0.29	0.19	−0.03	0.01	0.20	0.19
EDSS	−0.33	−0.36	−0.39	−0.46	−0.44	−0.44	−0.46	−0.56	−0.57	−0.55	−0.51	−0.50	−0.59	−0.50	−0.36	−0.22	−0.15	−0.45	−0.48
IPEC	0.07	0.06	−0.05	−0.09	−0.01	−0.01	0.07	0.02	−0.07	0.02	−0.04	−0.02	−0.02	0.02	0.03	0.05	0.06	0.00	0.00
AI	−0.46	−0.53	−0.54	−0.58	−0.58	−0.46	−0.46	−0.57	−0.65	−0.57	−0.59	−0.61	−0.72	−0.63	−0.49	−0.44	−0.34	−0.54	−0.57
DD	−0.66	−0.62	−0.63	−0.64	−0.61	−0.65	−0.61	−0.62	−0.58	−0.52	−0.51	−0.48	−0.47	−0.46	−0.32	−0.30	−0.32	−0.68	−0.49
PVL	−0.02	−0.14	−0.13	−0.14	−0.09	−0.24	−0.27	−0.30	−0.23	0.01	−0.19	−0.18	−0.04	−0.06	0.07	−0.01	−0.18	−0.17	−0.13
MS (*n*=18)																			
SNRS	0.62	0.65	0.61	0.58	0.52	0.56	0.49	0.66	0.61	0.61	0.71	0.70	0.63	0.65	0.53	0.49	0.23	0.63	0.64
EDSS	−0.75	−0.67	−0.63	−0.57	−0.51	−0.51	−0.44	−0.53	−0.54	−0.54	−0.52	−0.58	−0.58	−0.51	−0.45	−0.43	−0.28	−0.61	−0.55